Multiple-input Single-output Nonlinear System Identification using Bezier- Bernstein Polynomials with Noise Cancellation

Mohammad Jahani Moghaddam[1*]

Abstract- This article deals with an identification method for the fractional multiple-input single-output model. It is considered the Hammerstein model to separate dynamic linear and static nonlinear behaviors. Which Bezier-Bernstein polynomials are used to approximate the nonlinear functions and the fractional order transfer function is applied to estimate the linear part. A hybrid identification method based on a modified evolutionary algorithm and a recursive classic method is presented. As an advantage, this method can also correctly identify the system in the presence of output noise. A photovoltaic experimental system and a numerical example are used to illustrate the efficiency and performance of the proposed scheme.

Keywords: Nonlinear System Identification, Multi Input- Single Output Hammerstein Model, Bezier-Bernste in Polynomial, Modified Genetic Algorithm

1. Introduction

The utilization of fractional calculations has been observed in a variety of fields in science and technology, including image processing [1,2], signal processing [3], mechanics [4], path planning and tracking [5], control theory and applications [6], and real physical systems modeling and identification [7-12], etc. This supports the notion that real plants and processes inherently possess some degree of fractionality [6], thus requiring fractional-order models to yield more accurate and satisfactory identification results compared to integer models [7]. However, for systems with wide operating areas, nonlinear models such as neural networks, Volterra series, or block-oriented models should be considered [13].

The Hammerstein model is a sequential structure comprising a static nonlinear subsystem and a dynamic linear block. It has been widely utilized to identify various nonlinear systems across different engineering problems, including chemical processes [14], DC/DC converters [15], model-based controller design [16], speech signal processing [17], electric drives [18], electrically stimulated muscles [19], RF transmitters [20], and more.

The different literatures presented various identification algorithms for Hammerstein models that correspond to different applications [13, 21-26]. The various methods differ in how they represent memory less non-linear static parts and optimization algorithms used to approximate unknown parameters. A particular approach for identifying the Hammerstein model with commensurate fractional order transfer function as the linear part is proposed in [27], assuming the differential order is a known parameter. In [28], an iterative algorithm is presented to identify the continuous fractional order of the Hammerstein system in ARX and OE forms. This method applies only to nonlinear systems with quasi-linear properties and identifies two categories of linear and non-linear unknowns through least squares-based estimation in two steps. The P-type order learning algorithm is used iteratively to estimate the order of differentiation. Moreover, [29] proposes identifying the fractional order Wiener-Hammerstein model but faces issues such as initial guesses, mathematical complications, and making a large number of data assumptions. Reference [30] suggests identifying the fractional Hammerstein model by minimizing output error using the LM algorithm. Additionally, [31] uses Particle Swarm Optimization (PSO) to minimize output error.

One possibility to represent the static part is Bezier-Bernstein polynomials that are commonly utilized in computer design and graphics [32, 33]. In [32], an identification method based on the Bezier-Bernstein approximation single-input single-output (SISO) Hammerstein systems is proposed. However, this approach has several disadvantages that hinder its use in real-world nonlinear process identification, such as computational complexity and inaccurate estimation due to non-linear coefficient estimation using the Gauss-Newton algorithm, especially in noisy data. Ref. [34] considers the Hammerstein model in a multiple-input-single-output (MISO) structure and estimates both linear and non-linear parameters using the Levenberg-Marquardt (LM)

1* Corresponding author: Department of Electrical Engineering, Langarud Branch, Islamic Azad University, Langarud, Iran.

Email: Jahani.iaul@yahoo.com

Received: 2024.01.30; Accepted: 2024.04.30

algorithm. However, this article only focuses on estimating outputs of non-linear static parts. Both of these articles are based on integer Hammerstein model.

Prior methods of identification have not been able to adequately capture the nonlinearities present in the system. This issue stems mainly from utilizing a predetermined structure such as known-order polynomials, multi-segment piecewise linear forms, etc., for describing the nonlinear behavior of the system. In practical scenarios, it is often difficult to describe the characteristics of many plants using these predefined structures. The primary objective of this research paper is to propose a novel identification scheme for MISO fractional order Hammerstein models. Unlike previous approaches, we consider the form of nonlinear functions to be unknown and estimate them during the identification process. We use Bezier-Bernstein polynomials to estimate the static nonlinear component for this purpose. It has been demonstrated that among all polynomial functions utilized in function approximation, Bernstein basis is the most stable and best conditioned [35]. This provides an additional advantage to our application. Furthermore, we employ the Fractional Order Transfer Function (FOTF) to achieve a more precise estimation of the linear dynamic component.

The other sections of this article are prepared as follow: Section 2 provides a summary of fractional order transfer function mathematics background. Section 3 gives a brief introduction to Bezier-Bernstein polynomials. Section 4 contains my proposed identification method. Section 5 includes the numerical results and finally, the conclusion is explained in detail.

2. FRACTIONAL ORDER TRANSFER FUNCTION

A fractional differential equation (1) represents a dynamical continuous-time fractional system:

$$\begin{aligned} a_n D^{\alpha_n} y(t) + a_{n-1} D^{\alpha_{n-1}} y(t) + \cdots + a_0 D^{\alpha_0} y(t) = \\ = b_m D^{\beta_m} u(t) + b_{m-1} D^{\beta_{m-1}} u(t) + \cdots + b_0 D^{\beta_0} u(t) \end{aligned} \quad (1)$$

where the coefficients and fractional orders are denoted by $a_0, a_1, ..., a_n, b_0, b_1, ..., b_m \in R$ and $\alpha_0, \alpha_1, ..., \alpha_n, \beta_0, \beta_1, ..., \beta_m \in R$, respectively. The Riemann and Liouville arbitrary order differentiation is introduced as [12]:

$$D^{\alpha} = \left(\frac{d}{dt}\right)^{\alpha} \quad (2)$$

The Grünwald-Letnikov (GL) definition is used in this paper for simplicity of calculations. For $\alpha, a \in R, \alpha > 0$, GL formula of fractional derivative of order α (3), uses sampling step h and operating limits *a* and *t* of ${}_aD_t^{\alpha} f(t)$ [12]:

$${}_aD_t^{\alpha} f(t) = \lim_{h \to 0} \frac{1}{h^{\alpha}} \sum_{j=0}^{\left[\frac{t-a}{h}\right]} (-1)^j \binom{\alpha}{j} f(t - jh) \quad (3)$$

The binomial coefficients are calculated using the relationship between the factorial and the Euler gamma function [12]:

$$\binom{\alpha}{j} = \frac{\alpha!}{j!(\alpha - j)!} = \frac{\Gamma(\alpha + 1)}{\Gamma(j + 1)\Gamma(\alpha - j + 1)} \quad (4)$$

where the Euler Gamma function $\Gamma(.)$ is defined as [12]:

$$\Gamma(n) = \int_0^{\infty} t^{n-1} e^{-t} dt \quad (5)$$

Due to the existence of long memory behavior in fractional operator, Newton's binomial $\binom{\alpha}{j}$ rate of convergence to zero with j will be very slow, and in accordance with the principle of short memory for real implementation, an approximation of equation (2) using only recently past values of f(t) is defined as the simplest solution for the simulation of fractional systems in the time domain [36].

$$D^{\alpha} f(t) = \frac{1}{h^{\alpha}} \sum_{j=0}^{N} (-1)^j \binom{\alpha}{j} f(t - jh) \quad (6)$$

where $N = [T/h]$ is the approximation addends number [36].

The FOTF corresponding to Equation (1) is:

$$G(s) = \frac{Y(s)}{U(s)} = \frac{b_m s^{\beta_m} + b_{m-1} s^{\beta_{m-1}} + \cdots + b_0 s^{\beta_0}}{a_n s^{\alpha_n} + a_{n-1} s^{\alpha_{n-1}} + \cdots + a_0 s^{\alpha_0}} \quad (7)$$

3. BEZIER- BERNSTEIN POLYNOMIALS

The expanding of $[x + (1-x)]^d$ is formed the univariate Bernstein polynomial basis functions $B_{i,d}(x)$ defined as [33]:

$$B_{i,d}(x) = \binom{d}{i} x^i (1-x)^{d-i} \quad (8)$$

where *i* and *d* are nonnegative integers $i \le d$ over the region $x \in [0,1]$. The number of the single-variable Bernstein polynomials of order *d* is d + 1. Also, Bernstein polynomials are computed recursively:

$$B_{i,d}(x) = (1-x) B_{i,d-1}(x) + x B_{i-1,d-1}(x) \quad (9)$$

Bezier-Bernstein polynomials over the region [0,1] are defined as:

$$B_{i,n} f(t) = \sum_{i=0}^{n} \binom{n}{i} t^i (1-t)^{n-i} f\left(\frac{i}{n}\right), \quad n=1,2,.... \quad (10)$$

The Bezier-Bernstein polynomials over the [a, b] domain, which a, b are arbitrary numbers, are defined as:

$$B_{i,n}(t)=\binom{n}{i}\frac{(t-a)^{i}\,(b-t)^{n-i}}{(b-a)^{n}},\ \text{i=0,1,2,....,n} \quad (11)$$

4. THE IDENTIFICATION ALGORITHM

4.1. The Problem Statement

The fractional MISO Hammerstein model is constructed from a series of the nonlinear gain functions and FOTF as the dynamic part (Fig. 1) and is generally specified by:

$$y(t)=-\sum_{i=1}^{n}a_i D^{\alpha_i}y(t)+\sum_{j=0}^{m}b_j D^{\beta_j}(w_1(t)+...+w_k(t)) \quad (12)$$

where $w_k(t), k=1,2,...,r$ are the nonlinear gain functions outputs that entered to dynamic subsystem. The input and output delays for the dynamic part are denoted by n, m . In this paper, the nonlinear blocks are modelled as:

$$w_k(t)=f_k\left(u_k(t)\right)=\sum_{i=0}^{d}\delta_{ki}B_{ki,d}(u_k(t)) \quad (13)$$

where y(t) represents the system output, and $u_1,u_2,...,u_r$ represents the inputs. The Bezier-Bernstein polynomial associated to *k*th inputs are represented by $B_{ki,d}(u_k(t)), i=0,...,d, k=1,...,r$ and the corresponding weights are represented by $\delta_{ki}, i=0,1,\ldots,d, k=1,...,r$. Moreover, the dynamic part gain is determined by coefficients $a_1,...,a_n,b_0,...,b_m\in R$ and fractional orders $\alpha_1,...,\alpha_n,\beta_0,...,\beta_m\in R$ as:

$$G(s)=\frac{B(s)}{A(s)}=\frac{b_m s^{\beta_m}+\cdots+b_1 s^{\beta_1}+b_0 s^{\beta_0}}{1+a_n s^{\alpha_n}+\cdots+a_1 s^{\alpha_1}} \quad (14)$$

Based on equations (12), (13), the relationship between input and output can be expressed using the following equation:

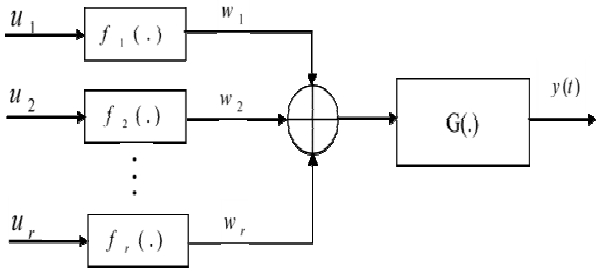

Fig. 1. The MISO Hammerstein model

$$y(t)=-\sum_{i=1}^{n}a_i D^{\alpha_i}y(t)+\sum_{j=0}^{m}b_j D^{\beta_j}(\sum_{k=0}^{d}\left(\delta_{1k}B_{1k,d}(u_1(t))+...\right.$$
$$\left.\ldots+\delta_{rk}B_{rk,d}(u_r(t))\right)) \quad (15)$$

Equation (15) is rewritten using the GL definition of fractional difference-integral as shown in equations (16) to (18) [36]:

$$y(k+1)=-\sum_{i=1}^{n}a_i' Y_i(k)+$$
$$+\sum_{j=0}^{m}\left(\sum_{g=0}^{d}b'_{1jg}(F_{1jg}(k))+...+\sum_{g=0}^{d}b'_{rjg}(F_{rjg}(k))\right) \quad (16)$$

$$a_i'=\frac{\frac{a_i}{h^{\alpha_i}}}{1+\sum_{k=1}^{n}\frac{a_k}{h^{\alpha_k}}},\quad b'_{wjg}=\frac{\frac{b_j(\delta w)_g}{h^{\beta_j}}}{1+\sum_{k=1}^{n}\frac{a_k}{h^{\alpha_k}}}, \quad (17)$$

$$1\le \text{i}\le \text{n},\ 1\le w\le r,\ 0\le g\le \text{d},\ 1\le j\le m$$

$$Y_i(k)=\sum_{j=1}^{N}(-1)^j\binom{\alpha_i}{j}y(k+1-j),$$

$$\text{F}_{\text{w}jg}(k)=\sum_{i=0}^{N}(-1)^i\binom{\beta_i}{j}\left(B_{wg,d}(u_w(k))\right), \quad (18)$$
$$,1\le w\le r, 0\le j\le d$$

By considering the actual inputs (*u(t)*) and measured outputs ($y^*(t)=y(t)+p(t)$), and defining Gaussian random noise $p(t)$ with zero mean and variance σ^2 , the equation (16) can be further rewritten as equation (19) [36].

$$y^*(k+1)=-\sum_{i=1}^{n}a_i' Y_i^*(k)+$$
$$+\sum_{j=0}^{m}\left(\sum_{g=0}^{d}b'_{1jg}(F_{1jg}(k))+...+\sum_{g=0}^{d}b'_{rjg}(Fr_{jg}(k))\right)+ \quad (19)$$
$$+e(k+1)$$

where:

$$Y_i^*(k)=\sum_{j=1}^{N}(-1)^j\binom{\alpha_i}{j}y^*(k+1-j) \quad (20)$$

$$e(k+1)=p(k+1)+\sum_{i=1}^{n}a_i'\sum_{j=1}^{N}(-1)^j\binom{\alpha_i}{j}p(k+1-j) \quad (21)$$

The unknown parameters in this model include the fractional orders $\alpha_1,...,\alpha_n,\beta_0,...,\beta_m$ and the coefficients of the transfer function $a_1,...,a_n,b_0,...,b_m$ and the weights of Bezier- Bernstein polynomials

$\delta_{k\,i}, i = 0,1,\ldots,d, k = 1,...,r$. To obtain these unknown parameters, this paper proposes the Modified Genetic Algorithm (MGA) [37] to identify the fractional orders α_i, β_j and provide an initial estimation for other unknown parameters a_i, b_j, δ_k . A recursive optimization algorithm is then used to update these other unknowns.

The cost function for this approach is the mean of squared output errors, as given in equation (22), where $y(k)$ is the real plant output and $y_{est}(k,\theta)$ is the estimated output, and *p* is the number of data samples.

$$e(\theta) = mean(y(k) - y_{est}(k,\theta))^2, k = 0,1,\ldots,p \quad (22)$$

Once the fractional orders are obtained, the recursive algorithm is applied to update the unknown coefficients and weights (a_i, b_j, δ_k) accordingly.

4.3. RLS Optimization Approach

The standard RLS algorithm requires an initial set of value samples to obtain the unique solution of the unknown parameter vector θ , which is determined by the dimension of the regressor ϕ . Equation (19) in the RLS form can be expressed as equation (23) which is linear with respect to the coefficients, where θ includes unknown parameters and $\phi(k)$ is the known vectors in *k*th step as shown in equations (24) and (25).

$$y(k+1) = \theta^T \phi(k) + e(k+1) \quad (23)$$

$$\theta = \left[a_1', \ldots, a_n', b_{100}^{'}, \ldots, b_{10d}^{'}, ..., b_{1m0}^{'}, \ldots, b_{1md}^{'}, \ldots \right.$$
$$\left. , ..., b_{r00}^{'}, \ldots, b_{r0d}^{'}, ..., b_{rm0}^{'}, \ldots, b_{rmd}^{'} \right]^T \quad (24)$$

$$\phi(k) = \left[-Y_1^*(k), \ldots, -Y_n^*(k), F_{100}(k), \ldots, F_{10d}(k), ..., F_{1m0}(k), \ldots \right.$$
$$\left. ..., F_{1md}(k), ..., F_{r00}(k), \ldots, F_{r0d}(k), ..., F_{rm0}(k), \ldots, F_{rmd}(k) \right]^T \quad (25)$$

The LS method provides a solution as equation (26) if the matrix $\left[\sum_{i=1}^{k} \phi(i-1)\phi^T(i-1) \right]^{-1}$ exists, but the matrix ϕ may become poorly conditioned or singular, making it difficult to calculate its inverse. To avoid this issue, MGA is used to obtain the required RLS initial values without needing to compute any inverses.

$$\hat{\theta}_k = \left[\sum_{i=1}^{k} \phi(i-1)\phi^T(i-1) \right]^{-1} \sum_{i=1}^{k} \phi(i-1) y(i) \quad (26)$$

Equation (27) is the recursive version of equation (26) and can be extended to online identification applications [36, 38, 39], where optimization results are updated in each iteration using new measured input/output.

$$\begin{cases} \hat{\theta}_{k+1} = \hat{\theta}_k + G_k \phi(k) \varepsilon(k+1) \\ G_{k+1} = G_k - \dfrac{G_k \phi(k) \phi^T(k) G_k}{1 + \phi^T(k) G_k \phi(k)} \\ \varepsilon(k+1) = \dfrac{y(k+1) - \hat{\theta}_k^T \phi(k)}{1 + \phi^T(k) G_k \phi(k)} \end{cases} \quad (27)$$

The adaptation gain matrix G for an initial value is generally selected according to equation (28) [36].

$$G_0 = \frac{1}{\gamma} I; \quad 0 < \gamma \ll 1 \quad (28)$$

The coefficients $a_i', i = 1,...,n$ are obtained from $\hat{\theta}$ directly and the assumption $b_0 = 1$ is used to calculate the values of $b_j \left(\delta_w\right)_g$, $1 \le w \le r,\ 0 \le g \le d,\ 1 \le j \le m$.

MGA estimates fractional orders ($\alpha_1,...,\alpha_n, \beta_0,...,\beta_m$) and produces initial estimations of other unknown parameters including $a_i', i = 1,...,n$ and $b_{w\,jg}^{'}, 1 \le w \le r, 0 \le g \le d, 1 \le j \le m$.

Where the multiplication of b_j s and $\left(\delta_w\right)_g$ s results in the unknown parameter beta $b_{w\,jg}^{'}$ s. These estimations are frequently updated by RLS. The $b_j, 1 \le j \le m$ coefficients and $b_{w\,jg}^{'}$ s are then used to calculate the weights of Bezier Bernstein polynomials $\left(\delta_w\right)_g, 1 \le w \le r, 0 \le g \le d$. If the stop conditions are satisfied, the identification process is complete. If not, RLS is applied again to reduce the estimation error. The identification process will continue until the desired accuracy is achieved.

5. SIMULATION RESULTS

To verify the effectiveness of the proposed approach, two examples are presented. The FOTF's general form is defined as the dynamic subsystem by equation (29).

$$G(s) = \frac{b_1 s^{\beta_1} + s^{\beta_0}}{a_2 s^{\alpha_2} + a_1 s^{\alpha_1} + a_0} \quad (29)$$

5.1. Example 1

In the first example, the real Photo-Voltaic (PV) module MF120EC3 is from Pusat Tenaga Malaysia (Malaysia Energy Centre, MEC) is taken into consideration [40].The inputs are Solar Irradiance (Ir) and Cell Temperature (CT), while the output is DC Current (DCC).The transfer function of the MISO PV system is expressed in equations (30) and (31) [40]. The Tustin estimation operator is used to obtain

the continuous versions of the transfer functions given by equations (32) and (33).

$$TF_{CT/DCC} = = \frac{.01358z^4 - .02393z^3 - .001419z^2 + .01159z}{z^4 - 1.148z^3 + 0.251z^2 - .01503z + .0381} \quad (30)$$

$$TF_{Ir/DCC} = = \frac{.05644z^4 - .06703z^3 - .002245z^2 + .00039z}{z^4 - 1.148z^3 + .251z^2 - .01503z + .0381} \quad (31)$$

$$TF_{CT/DCC} = = \frac{.009992s^4 + .1022s^3 + .1375s^2 - .05455s - .001168}{s^4 + 4.986s^3 + 9.341s^2 + 5.16s + .8226} \quad (32)$$

$$TF_{Ir/DCC} = = \frac{.04928s^4 + .2941s^3 + .5597s^2 + .2966s - .0812}{s^4 + 4.986s^3 + 9.341s^2 + 5.16s + .8226} \quad (33)$$

The proposed method involves generating a simulated MISO Hammerstein model using equations (32) and (33) and adding Gaussian noise $p(t) \in N(0, \sigma^2)$ with two various $\sigma^2 = 0.0001$ and $\sigma^2 = 0.01$ to the output. This method effectively cancels out the output noise. The inputs *CT* and *Ir* have uniform distributions within the ranges of $[20, 80]$ and $[0, 1000]$, respectively. To achieve optimal accuracy, MGA was utilized to determine the appropriate degree for the Bernstein basis function, starting from 3. Eventually, the polynomial degree was set to d = 5, using Equation (10) for the Bernstein polynomials, resulting in the generation of a sequence of regressors $B_{i,n}(u(t)), i = 0,1,...,5$. This generates a sequence of regressors and Bezier-Bernstein polynomial basis functions for each input, with 5 knots set for each input. For the first input, we set 5 knots at [20, 35, 50, 65, 80], and for the second input, we selected another set of 5 knots at [0, 250, 500, 750, 1000]. These knots generated 5 Bezier-Bernstein polynomial basis functions for each input that are depicted in Figs. 2- 5.

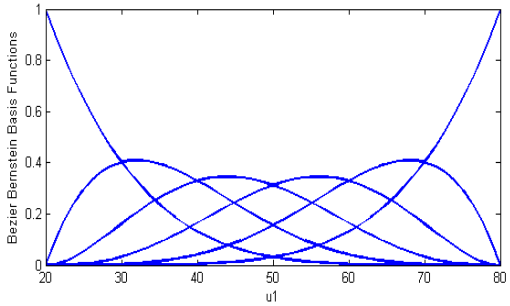

Fig. 2. Six Bezier–Bernstein polynomial basis functions constructed in Example 1 over the first input data u1

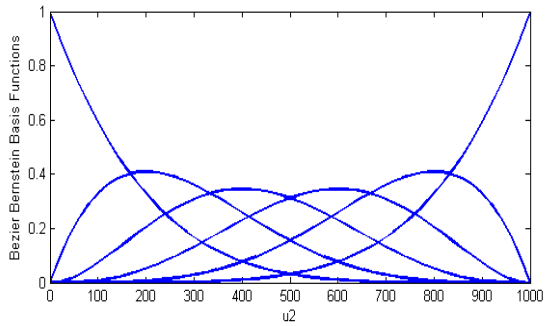

Fig. 3. Six Bezier–Bernstein polynomial basis functions constructed in Example 1 over the second input data u2.

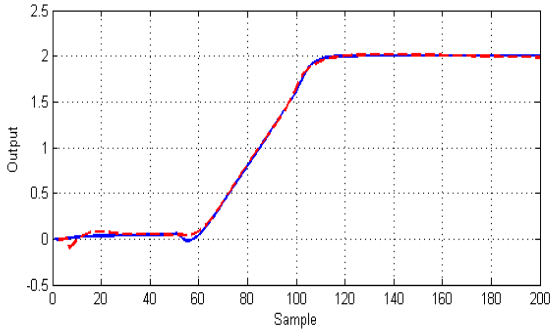

Fig. 4. The actual (blue line) and the estimated (red dashed line) outputs- PV Module ($\sigma^2 = 0.0001$)

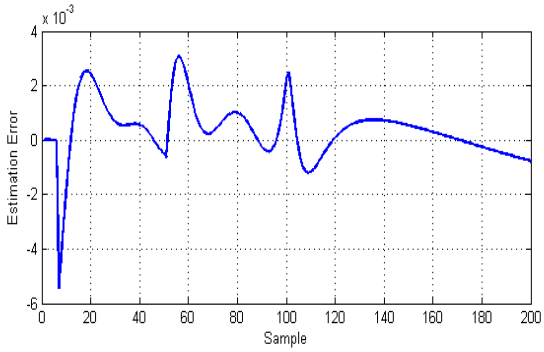

Fig. 5. The output estimation error- Example 1 ($\sigma^2 = 0.0001$)

The algorithm was iterated 200 times, reaching a Mean Squared Errors (MSE) value of for the clean output and for the noisy output. The estimated outputs and related errors are shown in Figs. 6, 7 for low noise and Figs. 9, 10 for high noise cases, demonstrating improved accuracy compared to reference [33]. The coefficients estimation using RLS is illustrated in Figs. 8, 11. The identified FOTFs are presented as (34) for low output noise and (35) for high output noise.

The algorithm was iterated over 200 cycles, resulting in a Mean Squared Error (MSE) value of 1.1857×10^{-6} for the low noise case and 2.4803×10^{-5} for the high noise measurements i.e., the noisy case. The estimated outputs and their corresponding estimation errors can be seen in Figs. 6, 7 and Figs. 9, 10 for the low and high noise cases, respectively. These results demonstrate an improvement in accuracy compared to the reference [33]. The coefficient

estimation process using RLS is shown in Figs. 8, 11 for both noise levels. The identified FOTFs for the low and high output noise cases are represented by Equations (34) and (35), respectively.

$$G(s)=\frac{s^{1.3461}-0.6257s^{0.0439}}{s^{1.2176}+2.5644s^{0.8157}+0.5815} \quad (34)$$

$$G(s)=\frac{2.4708s^{1.6082}+s^{0.0048}}{2.6007s^{0.9297}+s^{0.6486}+1.3365} \quad (35)$$

Tables 1 and 2 showcase a comparative analysis between fractional order and integer order transfer functions at two different levels of noise. Additionally, Table 2 compares the performance of MGA, classic GA, and PSO. The estimated outputs and corresponding errors using an integer order transfer function can be observed in Figs. 12-15. To prove the robustness of our proposed approach against input uncertainties, we introduced Gaussian noise $p(t)\in N(0,\sigma^2)$ with a standard deviation of $\sigma^2=0.01$ to the inputs of the Hammerstein model. Table 2 also presents the simulation results of this case, supporting our assertion that FOTF and MGA lead to superior identification accuracy.

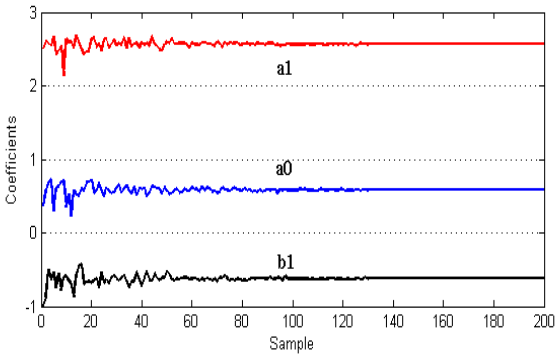

Fig. 6. RLS coefficients estimation process-PV Module ($\sigma^2=0.0001$)

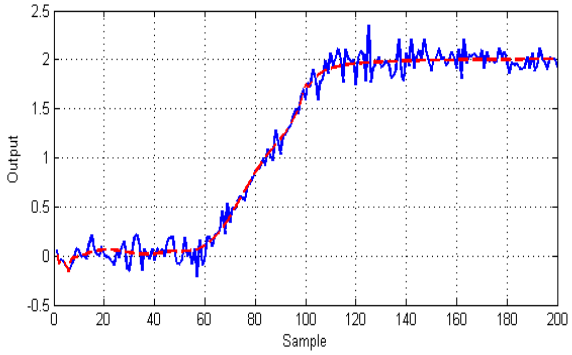

Fig. 7. The actual (blue line) and the estimated (red dashed line) outputs-PV Module ($\sigma^2=0.01$)

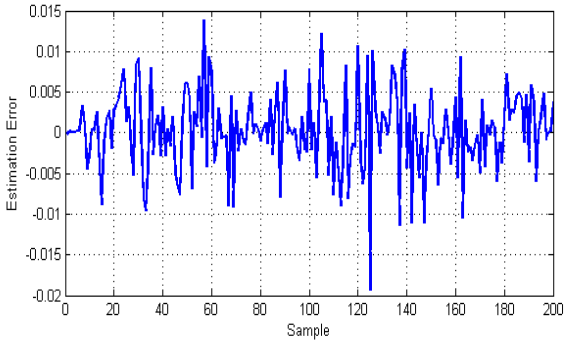

Fig. 8. The output estimation error-PV Module ($\sigma^2=0.01$)

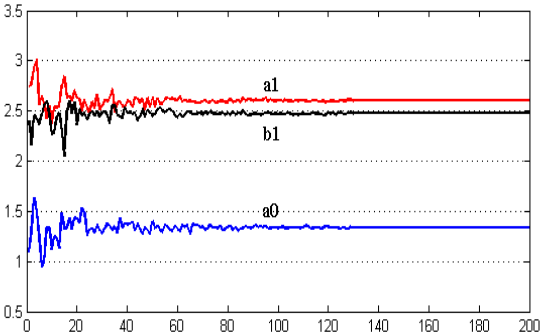

Fig. 9. RLS coefficients estimation process-PV Module ($\sigma^2=0.01$)

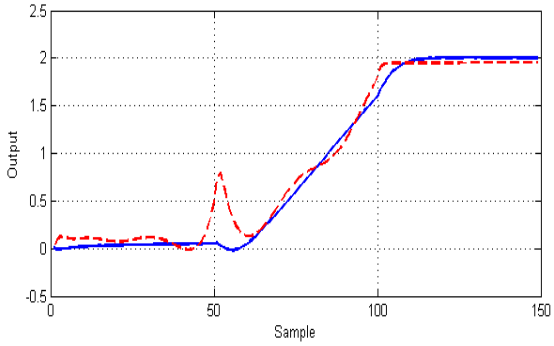

Fig. 10. The actual (blue line) and the estimated (red dashed line)outputs-integer order transfer function- PV Module($\sigma^2=0.0001$)

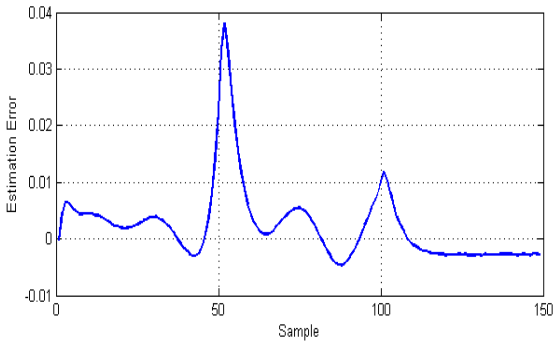

Fig. 11. The output estimation error-integer order transfer function -PV Module($\sigma^2=0.0001$)

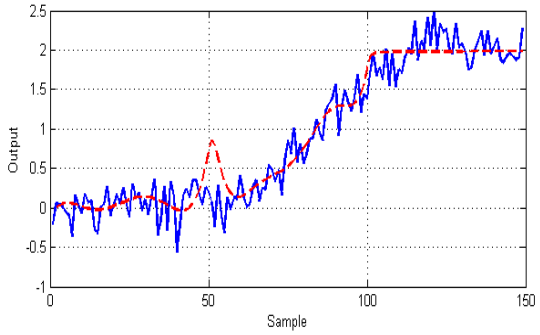

Fig. 12. The actual (blue line) and the estimated (red dashed line)outputs- integer order transfer function- PV Module ($\sigma^2 = 0.01$)

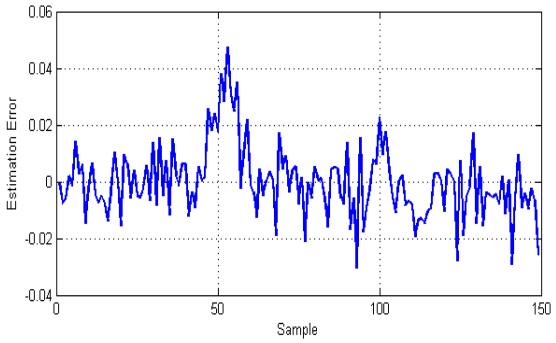

Fig. 13.The output estimation error- integer order transfer function -PV Module($\sigma^2 = 0.01$)

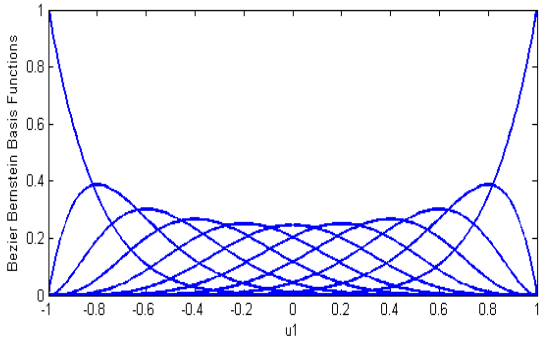

Fig. 14. Eleven Bezier–Bernstein polynomial basis functions constructed in Example 2 over the first input data u1

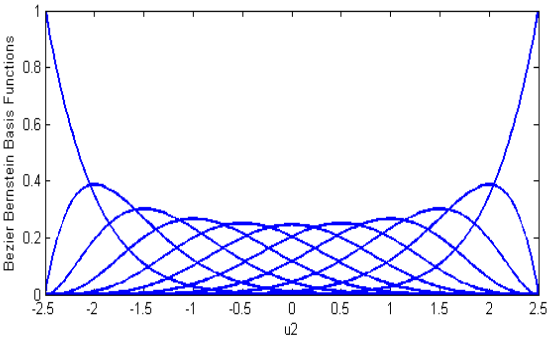

Fig. 15. Eleven Bezier–Bernstein polynomial basis functions constructed in Example 2 over the second input data u2

Table 1. The estimation error comparison between two different linear parts in PV Module ($\sigma^2 = 0.0001$).

Approach	MSE	RMS
Integer Order Transfer Function	4.1182×10^{-5}	0.0073
Fractional Order Transfer Function	1.1857×10^{-6}	0.0018

Table 2. The estimation error comparison between different optimization approaches and with two different linear parts in PV Module ($\sigma^2 = 0.01$).

Approach			MSE	RMS
PSO & RLS			$1.3886\times10^{-}$	0.011723
GA & RLS			1.2601×10^{-4}	0.011637
MGA & RLS	Integer Order Transfer Function		1.3777×10^{-4}	0.012102
	Fractional Order Transfer Function	Without Input Noise	$2.4803\times10^{-}$	0.004305
		With Input Noise	$5.9813\times10^{-}$	0.008000

5.2. Example 2

The Steam-Water Heat Exchanger (SWHE) nonlinear gain function [34] is used as a numerical example in the second case. Eq. (36) describes the SWHE which has been studied previously in [41], whereas $f_2(u)$ in Eq. (37) represents its nonlinear gain function. To create a MISO system, $f_1(u)$ is incorporated into the system model. The function $sat(x, x_-, x_+)$ is the saturation function with respective left and right breaking points in x_- and x_+ [34].

$$y(t) = 1.608y(t-1) - 0.6385y(t-2) + 0.3f_1(u_1(t)) + \\ + 0.207f_2(u_2(t-1)) - 0.1764f_2(u_2(t-2)) + p(t) \quad (36)$$

$$f_1(u) = sat(u, -0.6, 0.6)$$

$$f_2(u) = -31.549u + 41.732u^2 - 24.201u^3 + 68.634u^4 \quad (37)$$

Gaussian noise $p(t) \in N(0, \sigma^2)$ with different $\sigma^2 = 0.0001$ and $\sigma^2 = 0.01$ values is added to the Hammerstein model to demonstrate the proposed method's ability to eliminate output noise. The intervals [-1, 1] and [-2.5, 2.5] set the input limits for u_1 and u_2, respectively. In order to achieve accurate results, MGA is implemented to

determine the appropriate degree of Bernstein basis functions. Consequently, 11 knots are selected for each input, producing 11 Bezier-Bernstein polynomial basis functions for each input as demonstrated in Figs. 16 and 17. The 11 knots for the first input was set as [-1, -0.8, -0.6, -0.4, -0.2, 0, 0.2, 0.4, 0.6, 0.8, 1] and a set of 11 knots for the second input were selected as [-2.5, -2, -1.5, -1, -0.5, 0, 0.5, 1, 1.5, 2, 2.5]. Finally, one hundred input/output data samples are generated using Eqs. (36) and (37).

And as a result, aset of In the case of $\sigma^2 = 0.0001$, MSE after 100 iteration cycles became 1.8646×10^{-5}. The estimation of dynamic subsystem is obtained as:

$$G(s) = \frac{0.2880s^{0.5594} + s^{0.8616}}{3.9933s^{2.3921} + 4.7773s^{0.4164} + 2.4674} \quad (38)$$

In the case of a rather noisy data, i.e. $\sigma^2 = 0.01$, after 100 iterations, the MSE value was equaled to 5.3781×10^{-5}. The dynamic transfer function is obtained as:

$$G(s) = \frac{4.6881s^{0.3307} + s^{0.0526}}{2.6694s^{3.4542} + 4.5400s^{0.5089} + 2.1056} \quad (39)$$

Figures 16-19 display the estimation accuracy of nonlinear static parts and corresponding errors. Additionally, Figures 21 and 23 provide a visual representation of outputs approximated with low and high noise levels, respectively, with their related errors depicted in Figures 22 and 24. Furthermore, Figures 20 and 25 illustrate coefficients estimation using RLS for two distinct amounts of noise.

For this particular experiment, a comparison was carried out between fractional order and integer order transfer functions as linear dynamic parts. Tables 3 and 4 present results for two different noise levels, with estimated outputs and corresponding errors depicted in Figures 26-29. The optimization method employed significantly improved estimation accuracy compared to the GA and PSO methods, as showcased in Table 4. Moreover, the proposed method's robustness against input uncertainty was demonstrated by introducing Gaussian noise $p(t) \in N(0,\sigma^2)$ with standard deviation $\sigma^2 = 0.01$ to each model input, as shown in Table 4. Finally, Tables 3 and 4 highlight the superior identification accuracy achieved using FOTF and MGA.

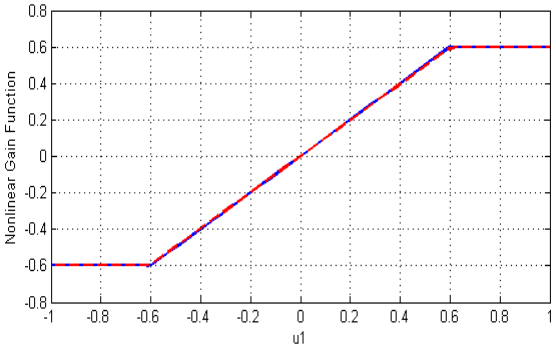

Fig. 16. The actual (blue line) and the estimated (red dashed line)nonlinear gain functions associated with the first input in low noise condition(SWHE)

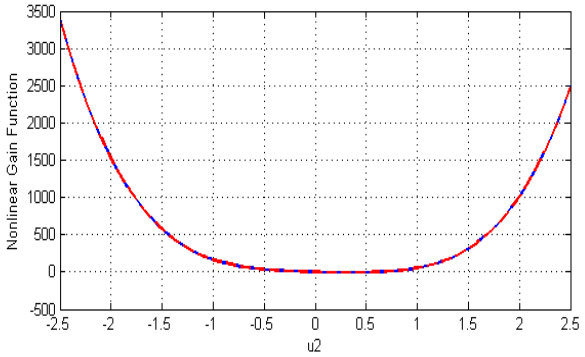

Fig. 17. The actual (blue line) and the estimated (red dashed line) nonlinear gain functions associated with the second input in low noise condition (SWHE)

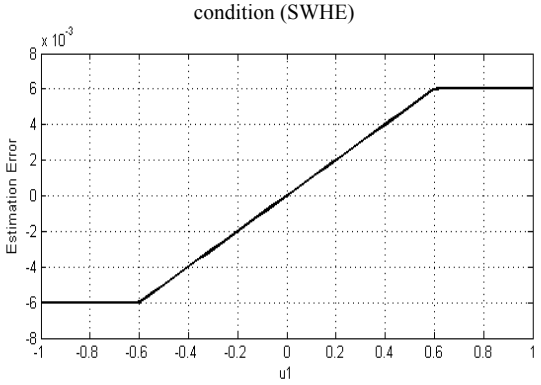

Fig. 18. Corresponding estimation errors regarding the first nonlinear function (SWHE)

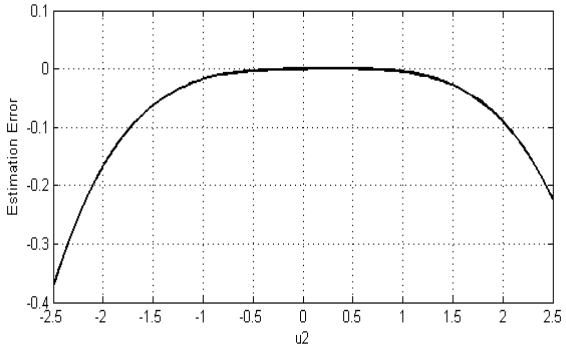

Fig. 19. Corresponding estimation errors regarding the second nonlinear function (SWHE)

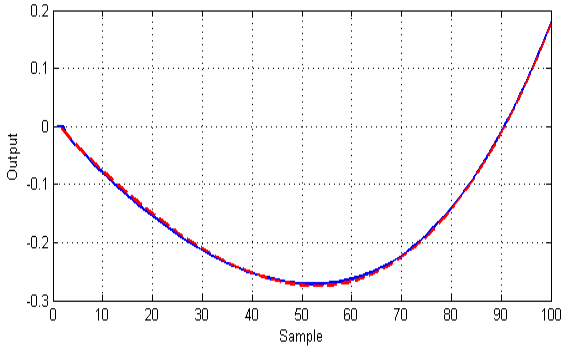

Fig. 20. The actual output (blue line) and the estimated output (red dashed line)-SWHE ($\sigma^2 = 0.0001$)

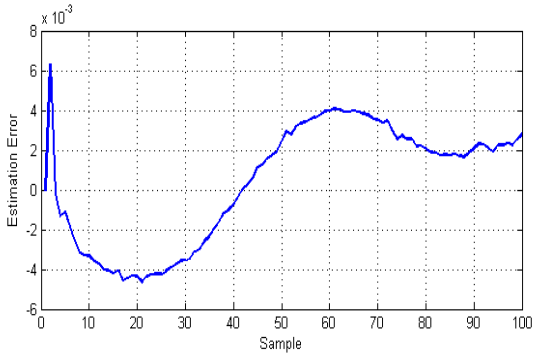

Fig. 21. The output estimation error- SWHE ($\sigma^2 = 0.0001$)

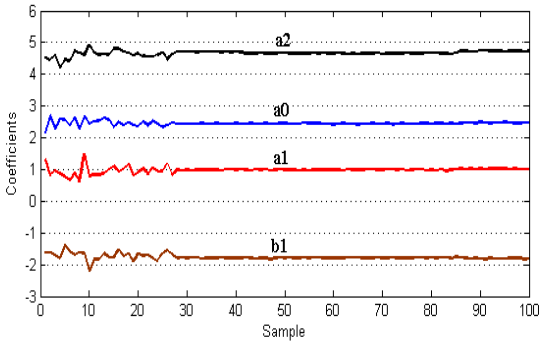

Fig. 22. RLS coefficients estimation regarding SWHE ($\sigma^2 = 0.0001$)

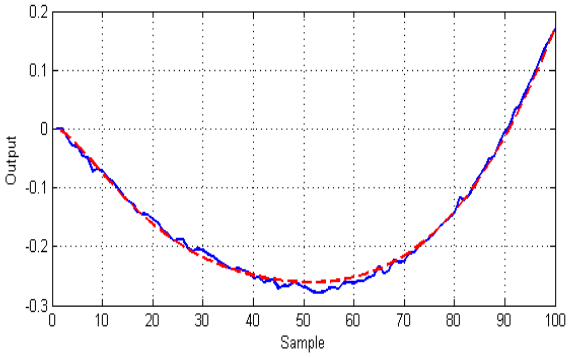

Fig. 23. The actual (blue line) and the estimated (red dashed line) outputs regarding SWHE ($\sigma^2 = 0.01$)

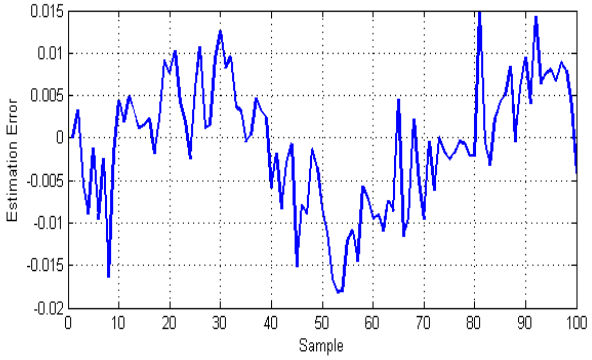

Fig. 24. The output estimation error-SWHE ($\sigma^2 = 0.01$)

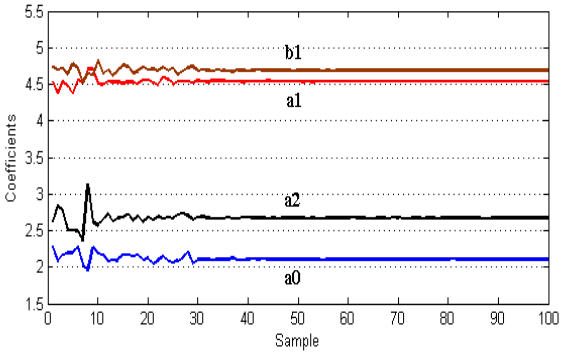

Fig. 25. RLS coefficients estimation regarding SWHE ($\sigma^2 = 0.01$)

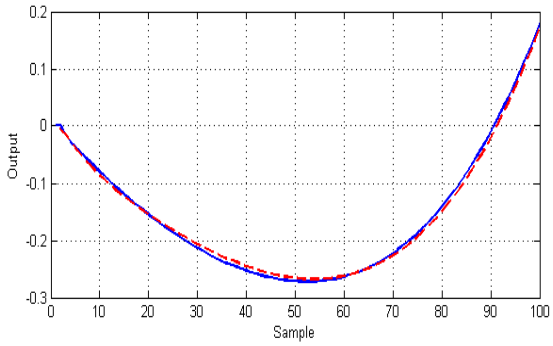

Fig. 26. The actual (blue line) and the estimated (red dashed line) outputs-integer order transfer function-SWHE ($\sigma^2 = 0.0001$)

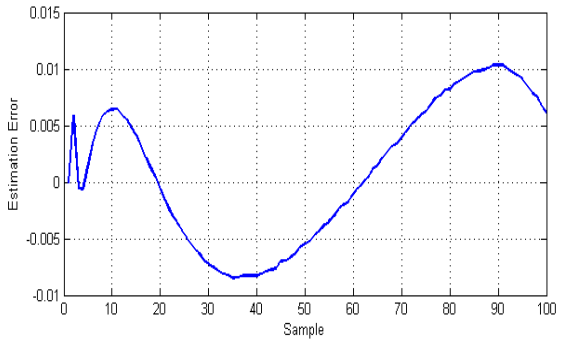

Fig. 27. The output estimation error- integer order transfer function-SWHE($\sigma^2 = 0.0001$)

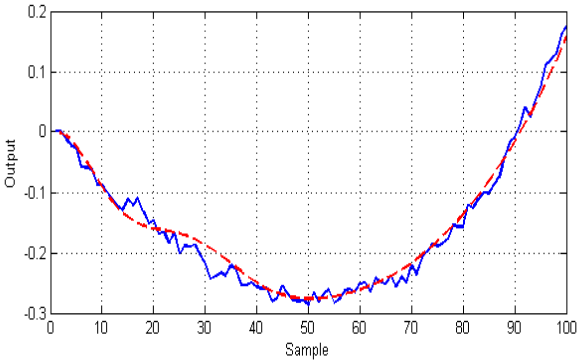

Fig. 28. The actual (blue line) and the estimated (red dashed line) outputs-integer order transfer function-SWHE($\sigma^2 = 0.01$)

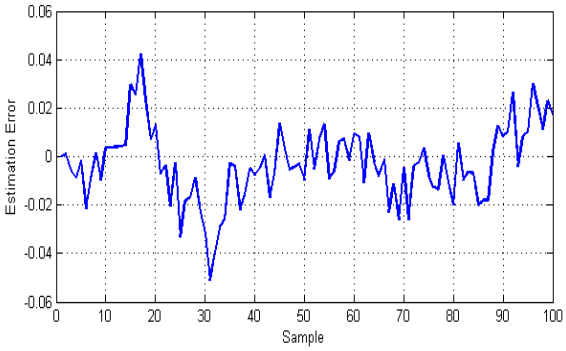

Fig. 29. The output estimation error- integer order transfer function-SWHE ($\sigma^2 = 0.01$)

Table 3. The estimation errorcomparison between two different linear parts in SWHE ($\sigma^2 = 0.0001$).

Approach	MSE	RMS
Integer Order Transfer Function	3.5895×10^{-4}	0.0104
Fractional Order Transfer Function	1.8646×10^{-5}	0.0019

Table 4. The output estimation errorcomparison between two different optimization approaches and with two different linear parts in SWHE ($\sigma^2 = 0.01$).

Approach			MSE	RMS
PSO & RLS			3.2069×10^{-4}	0.0151
GA & RLS			1.7230×10^{-4}	0.0122
MGA & RLS	Integer Order Transfer Function		5.7775×10^{-4}	0.0157
	Fractional Order Transfer Function	Without Input Noise	5.3781×10^{-5}	0.0054
		With Input Noise	8.2548×10^{-5}	0.0088

6. CONCLUSIONS

The study presented a novel approach for the identification of Multiple-Input Single-Output (MISO) fractional order Hammerstein models using Bezier-Bernstein polynomials with noise cancellation. Through comprehensive simulation results and analysis on the presented PV module and SWHE case studies, we have demonstrated the effectiveness and robustness of the proposed method in accurately capturing the complex nonlinear behaviors of the systems while mitigating the impact of output noise. The achieved results showcase superior identification performance and noise cancellation capabilities, laying the foundation for advancements in nonlinear system identification methodologies.

Looking ahead, future research endeavors could extend this method to more diverse and complex practical systems, exploring its applicability in real-world scenarios. Furthermore, the application of this method in other domains such as control systems, robotics, and industrial processes presents an exciting avenue for further investigation. Additionally, research efforts could focus on refining the algorithm's efficiency and extending its capabilities to address broader classes of nonlinear systems, thus contributing to a more comprehensive understanding and utilization of fractional order models in practical engineering applications

Statements & Declarations

Funding

The authors declare that no funds, grants, or other support were received during the preparation of this manuscript.

Competing Interests

The authors have no relevant financial or non-financial interests to disclose.

Data Availability Statement

The examples data are available in references [34, 40].The data that support the findings of this study are available from the corresponding author upon reasonable request.

Author Contributions

Study concept and design; analysis and interpretation of data**;** drafting of the manuscript**;** critical revision of the manuscript for important intellectual content; and statistical analysis are all done by the corresponding author.

REFERENCES

[1] Birs, I. R., Muresan, C. I., Folea, S., & Prodan, O. (2016). A comparison between integer and fractional order pd controllers for vibration suppression. Applied Mathematics and Nonlinear Sciences, 1(1), 273-282.

[2] Yang Q, Chen D, Zhao T, Chen Y. Fractional calculus in image processing: a review. Fractional Calculus and Applied Analysis. 2016 Oct 1;19(5):1222-49.

[3] Sheng H, Chen Y, Qiu T. An Overview of Fractional Processes and Fractional-Order Signal Processing Techniques. In Fractional Processes and Fractional-Order Signal Processing 2012 (pp. 31-46). Springer London. ISBN: 978-1-4471-2232-6

[4] Baleanu D, Golmankhaneh AK, Nigmatullin R, Golmankhaneh AK. Fractional newtonian mechanics. Central European Journal of Physics. 2010 Feb 1;8(1):120-125.

[5] Yousfi N, Melchior P, Rekik C, Derbel N, Oustaloup A. Path tracking design by fractional prefilter using a combined QFT/H∞ design for TDOF uncertain feedback systems. J. Appl. Nonlinear Dyn. 2012;1(3):239-61.

[6] Monje CA, Vinagre BM, Feliu V, Chen Y. Tuning and auto-tuning of fractional order controllers for industry applications. Control engineering practice. 2008 Jul 31;16(7):798-812.

[7] Gabano JD, Poinot T, Kanoun H. Identification of a thermal system using continuous linear parameter-varying fractional modelling. IET Control Theory & Applications. 2011 May 5;5(7):889-99.
[8] Cois O, Oustaloup A, Battaglia E, Battaglia JL. Non integer model from modal decomposition for time domain system identification. IFAC Proceedings Volumes. 2000 Jun 30;33(15):989-94.
[9] Poinot T, Trigeassou JC. Identification of fractional systems using an output-error technique. Nonlinear Dynamics. 2004 Dec 1;38(1):133-54.
[10] Lin J, Poinot T, Li ST, Trigeassou JC. Identification of non-integer-order systems in frequency domain. Journal Control Theory Appl.2008;25:517-20.
[11] Valerio D, Sa da Costa J. Identifying digital and fractional transfer functions from a frequency response. International Journal of Control. 2011 Mar 1;84(3):445-57.
[12] Petras I. Fractional-order nonlinear systems: modeling, analysis and simulation. Springer Science & Business Media; 2011 May 30. ISBN: 978-3-642-18100-9.
[13] Ivanov DV. Identification discrete fractional order Hammerstein systems. In Control and Communications (SIBCON), 2015 International Siberian Conference on 2015 May 21 (pp. 1-4). IEEE.
[14] Rattanawaorahirunkul R, Sanposh P, Panjapornpon C. Nonlinear system identification of pH process using Hammerstein-Wiener model. InElectronics, Information, and Communications (ICEIC), 2016 International Conference on 2016 Jan 27 (pp. 1-4). IEEE.
[15] Alonge F, D'Ippolito F, Raimondi FM, Tumminaro S. Nonlinear modeling of DC/DC converters using the Hammerstein's approach. IEEE transactions on power electronics. 2007 Jul;22(4):1210-21.
[16] Huo HB, Zhu XJ, Hu WQ, Tu HY, Li J, Yang J. Nonlinear model predictive control of SOFC based on a Hammerstein model. Journal of Power Sources. 2008 Oct 15;185(1):338-44.
[17] Turunen J, Tanttu JT, Loula P. Hammerstein model for speech coding. EURASIP Journal on Applied Signal Processing. 2003 Jan 1;2003:1238-49.
[18] Balestrino A, Landi A, Ould-Zmirli M, Sani L. Automatic nonlinear auto-tuning method for Hammerstein modeling of electrical drives. IEEE Transactions on Industrial Electronics. 2001 Jun;48(3):645-55.
[19] Le F, Markovsky I, Freeman CT, Rogers E. Recursive identification of Hammerstein systems with application to electrically stimulated muscle. Control Engineering Practice. 2012 Apr 30;20(4):386-96.
[20] Taringou F, Hammi O, Srinivasan B, Malhame R, Ghannouchi F M, Behaviour modelling of wideband RF transmitters using Hammerstein–Wiener models, IET circuits, devices & systems, 2010, 4(4), 282--290.
[21] Bai EW, Fu M. A blind approach to Hammerstein model identification. IEEE Transactions on Signal Processing. 2002 Jul;50(7):1610-9.
[22]Hasiewicz Z, Mzyk G. Hammerstein system identification by non-parametric instrumental variables. International Journal of Control. 2009 Mar 1;82(3):440-55.
[23] Greblicki W. Stochastic approximation in nonparametric identification of Hammerstein systems. IEEE Transactions on Automatic Control. 2002 Nov;47(11):1800-10.
[24] Chen H F, Pathwise convergence of recursive identification algorithms for Hammerstein systems, IEEE Transactions on Automatic Control, 2004, 49(10), 1641--1649.
[25] Goethals I, Pelckmans K, Suykens JA, De Moor B. Subspace identification of Hammerstein systems using least squares support vector machines. IEEE Transactions on Automatic Control. 2005 Oct;50(10):1509-19.
[26] Mete S, Ozer S, Zorlu H. System identification using Hammerstein model optimized with differential evolution algorithm. AEU-International Journal of Electronics and Communications. 2016 Dec 31;70(12):1667-75.
[27] Mohamed AO, Malti R, Olivier CO, Oustaloup A. System Identification Using Fractional Hammerstein Models. IFAC Proceedings Volumes. 2002 Dec 31;35(1):265-9.
[28] Zhao Y, Li Y, Chen Y. Complete parametric identification of fractional order Hammerstein systems. InFractional Differentiation and Its Applications (ICFDA), 2014 International Conference on 2014 Jun 23 (pp. 1-6). IEEE.
[29] Vanbeylen L. A fractional approach to identify Wiener–Hammerstein systems. Automatica. 2014 Mar 31;50(3):903-9.
[30] Hammar K, Djamah T, Bettayeb M. Fractional Hammerstein system identification using polynomial non-linear state space model. InControl, Engineering & Information Technology (CEIT), 2015 3rd International Conference on 2015 May 25 (pp. 1-6). IEEE.
[31] Hammar K, Djamah T, Bettayeb M. Fractional hammerstein system identification using particle swarm optimization. InModelling, Identification and Control (ICMIC), 2015 7th International Conference on 2015 Dec 18 (pp. 1-6). IEEE.
[32] Hong X, Mitchell RJ. Hammerstein model identification algorithm using Bezier–Bernstein approximation. IET Control Theory & Applications. 2007 Jul 1;1(4):1149-59.
[33] Farin G. Curves and surfaces for computer-aided geometric design: a practical guide. Elsevier; 2014 Jun 28.
[34] Ahmadi M, Mojallali H. Identification of multiple-input single-output Hammerstein models using Bezier curves and Bernstein polynomials. Applied Mathematical Modelling. 2011 Apr 30;35(4):1969-82.
[35] Farouki R, Goodman T. On the optimal stability of the Bernstein basis. Mathematics of Computation of the American Mathematical Society. 1996;65(216):1553-66.
[36] Jahani Moghaddam, M., Mojallali, H., &Teshnehlab, M. (2018). Recursive identification of multiple-input single-output fractional-order Hammerstein model with time delay. Applied Soft Computing, 70, 486-500.
[37] Jahani Moghaddam, M., Mojallali, H., &Teshnehlab, M. (2018). A multiple-input–single-output fractional-order Hammerstein model identification based on modified

neural network. Mathematical Methods in the Applied Sciences, 41(16), 6252-6271.
[38] Sundari S, Nachiappan A. Online Identification Using RLS Algorithm and Kaczmarz's Projection Algorithm for a Bioreactor Process. International Journal of Engineering and Computer Science. 2014;3:7974-8.
[39] Vahidi A, Stefanopoulou A, Peng H. Recursive least squares with forgetting for online estimation of vehicle mass and road grade: theory and experiments. Vehicle System Dynamics. 2005 Jan 1;43(1):31-55.
[40] Hussain MN, Omar AM, Samat AA. Identification of multiple input-single output (miso) model for mppt of photovoltaic system. InControl System, Computing and Engineering (ICCSCE), 2011 IEEE International Conference on 2011 Nov 25 (pp. 49-53). IEEE.
[41] Eskinat E, Johnson SH, Luyben WL. Use of Hammerstein models in identification of nonlinear systems. AIChE Journal. 1991 Feb 1;37(2):255-68.